

# Low-Range-Sidelobe Waveform Design for MIMO-OFDM ISAC Systems

Peishi Li<sup>†</sup>, Zichao Xiao<sup>†</sup>, Ming Li<sup>†</sup>, Rang Liu<sup>‡</sup>, and Qian Liu<sup>§</sup>

<sup>†</sup> School of Information and Communication Engineering

Dalian University of Technology, Dalian, Liaoning 116024, China

E-mail: {lpeishi, xiaozichao}@mail.dlut.edu.cn, mli@dlut.edu.cn

<sup>‡</sup> Center for Pervasive Communications and Computing

University of California, Irvine, CA 92697, USA

E-mail: rangl2@uci.edu

<sup>§</sup> School of Computer Science and Technology

Dalian University of Technology, Dalian, Liaoning 116024, China

E-mail: qianliu@dlut.edu.cn

**Abstract**—Integrated sensing and communication (ISAC) is a promising technology in future wireless systems owing to its efficient hardware and spectrum utilization. In this paper, we consider a multi-input multi-output (MIMO) orthogonal frequency division multiplexing (OFDM) ISAC system and propose a novel waveform design to provide better radar ranging performance by taking range sidelobe suppression into consideration. In specific, we aim to design the MIMO-OFDM dual-function waveform to minimize its integrated sidelobe level (ISL) while satisfying the quality of service (QoS) requirements of multi-user communications and the transmit power constraint. To achieve a lower ISL, the symbol-level precoding (SLP) technique is employed to fully exploit the degrees of freedom (DoFs) of the waveform design in both temporal and spatial domains. An efficient algorithm utilizing majorization-minimization (MM) framework is developed to solve the non-convex waveform design problem. Simulation results reveal radar ranging performance improvement and demonstrate the benefits of the proposed SLP-based low-range-sidelobe waveform design in ISAC systems.

**Index Terms**—Integrated sensing and communication (ISAC), waveform design, range sidelobe, symbol-level precoding (SLP).

## I. INTRODUCTION

Integrated sensing and communication (ISAC) has gained widespread attention from both industry and academia since it has been deemed as a key technique in future wireless networks and autonomous vehicular systems [1]. The crucial challenge in ISAC systems lies in the dual-functional waveform design that should balance the performance requirements of both communication and sensing [2]. Multi-input multi-output (MIMO) orthogonal frequency division multiplexing (OFDM) has been widely adopted in various wireless systems, owing to its superior ability of providing high-performance wireless communications. Consequently, the utilization of MIMO-OFDM waveform to achieve both communication and sensing functions is one of the most proposing approaches to deploy ISAC in practical networks. Numerous dual-function MIMO-OFDM waveform designs have been proposed by jointly considering different communication and sensing performance metrics to achieve a satisfactory performance trade-

off. Typical sensing performance metrics include the signal-to-interference-plus-noise ratio (SINR) at the radar receiver [3], the mean squared error (MSE) of the beampattern [4], the Cramér-Rao bound (CRB) [5], etc.

The above-mentioned waveform designs mainly focus on the spatial second-order statistics of the transmitted waveforms, which attempt to improve radar sensing performance while enabling beamforming gains for communications. Ironically, the randomness of communication information causes the ISAC dual-function waveform to inherently exhibit a high range sidelobe level, which may severely degrade the radar ranging performance. However, existing dual-function waveform designs ignore the range sidelobe, which is a crucial factor for radar ranging performance. To mitigate range sidelobes, many deterministic sequences that exhibit good aperiodic auto/cross-correlation properties are introduced for radar waveform designs [6]. Therefore, a low-range-sidelobe waveform design is becoming a crucial task for ISAC systems.

Fortunately, the recently-emerged symbol-level precoding (SLP) technique, which fully exploits the degrees of freedom (DoFs) of both spatial and temporal domains, can be utilized for low-range-sidelobe waveform designs in MIMO-OFDM ISAC systems. Particularly, by elaborately designing the waveform in each symbol time-slot, the SLP technique can efficiently suppress the range sidelobes and improve the radar ranging performance. On the other hand, from the perspective of multi-user communications, the SLP technique can utilize the symbol information to convert the harmful multi-user interference (MUI) into constructive interference (CI), thus achieving better communication quality of service (QoS). Therefore, SLP is a promising solution to improve the performance of dual-function waveforms in both communication and sensing functions by fully exploiting the DoFs in both spatial and temporal domains. To the best of our knowledge, SLP-based low-range-sidelobe waveform designs for ISAC systems have not been investigated in the existing literature.

In this paper, we investigate the SLP-based low-range-

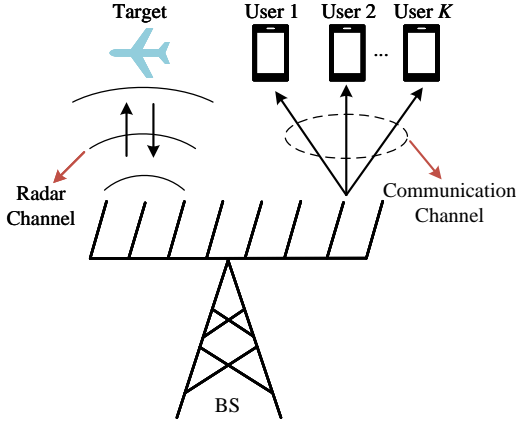


Fig. 1: An MIMO-OFDM ISAC system.

sidelobe waveform design for an MIMO-OFDM ISAC system, where a multi-antenna base station (BS) performs both down-link multi-user communication and radar sensing functions. In particular, we optimize the SLP-based MIMO-OFDM waveform to minimize the integrated sidelobe level (ISL) of the transmit waveform to suppress its range sidelobe while satisfying the multi-user communication QoS requirements and the transmit power constraint. We develop an efficient algorithm utilizing the majorization-minimization (MM) framework to solve the resulting non-convex waveform design problem, which exploits the unique signal structures, significantly reducing the computational complexity. Finally, simulation results are provided to reveal radar ranging performance improvement and validate the benefits of the proposed SLP-based low-range-sidelobe waveform design in ISAC systems.

## II. SYSTEM MODEL AND PROBLEM FORMULATION

### A. Transmitted Signal Model

The considered ISAC system is illustrated in Fig. 1. We assume that the BS is equipped with  $N_t$  transmit antennas in a uniform linear array (ULA) and serves  $K$  single-antenna communication users while sensing one target with range  $R$  in angle  $\theta$  using OFDM signals with  $N$  subcarriers. In specific, the transmitted symbol vector on the  $n$ -th subcarrier in the  $l$ -th time-slot is denoted as  $\mathbf{s}_n[l] \triangleq [s_{n,1}[l], s_{n,2}[l], \dots, s_{n,K}[l]]^T \in \mathbb{C}^K$ . The corresponding SLP transmit waveform  $\mathbf{x}_n[l] \in \mathbb{C}^{N_t}$  is designed to realize functions of delivering information  $\mathbf{s}_n[l]$  to  $K$  users and sensing the target.

With  $\Delta f$  denoting the subcarrier spacing, and  $f_c$  the carrier frequency, the transmitted signal is expressed as

$$\mathbf{x}(t) = \frac{1}{\sqrt{N}} \sum_{n=0}^{N-1} \mathbf{x}_n[l] e^{j2\pi(f_c + n\Delta f)t}, \quad (1)$$

where  $t \in [(l-1)(T_s + T_{cp}) + T_{cp}, l(T_s + T_{cp})]$ ,  $\forall l$ ,  $T_s$  is the OFDM symbol duration, and  $T_{cp}$  is the cyclic prefix (CP) duration.

### B. Multi-user Communication Model

To simplify the description of SLP, we assume that the modulated symbol  $s_{n,k}[l]$  is obtained by  $\Omega$ -phase-shift-keying

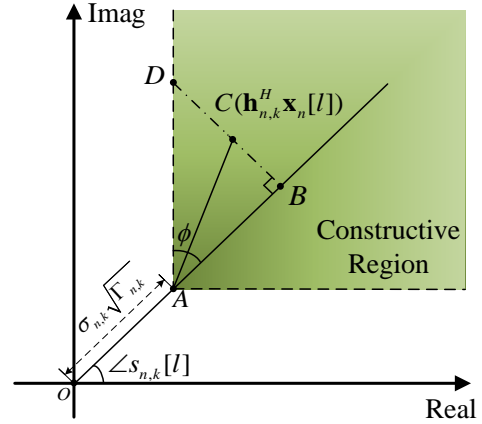


Fig. 2: The idea of CI for a QPSK symbol.

(PSK) ( $\Omega = 2, 4, \dots$ ). The corresponding SLP transmit waveform  $\mathbf{x}_n[l]$  is designed to transfer information  $s_{n,k}[l]$  to the communication users. The channel impulse response from the BS to the  $k$ -th user can be modeled by a tapped delay line (TDL) with  $U$  taps  $\{\bar{\mathbf{h}}_{1,k}, \dots, \bar{\mathbf{h}}_{u,k}\}$  [7], where  $\bar{\mathbf{h}}_{u,k} \in \mathbb{C}^{N_t}$  is assumed to be perfectly known at the BS. Then, the received signal on the  $n$ -th subcarrier at the  $k$ -th user is given by

$$y_{n,k}[l] = \mathbf{h}_{n,k}^H \mathbf{x}_n[l] + z_{n,k}, \quad (2)$$

where  $\mathbf{h}_{n,k} \in \mathbb{C}^{N_t}$  denotes the frequency-domain channel, and  $z_{n,k} \sim \mathcal{CN}(0, \sigma^2)$  is the additive white Gaussian noise (AWGN).

SLP converts the harmful MUI into CI by elaborately designing the transmit waveform  $\mathbf{x}_n[l]$  based on the transmitted symbol  $s_{n,k}[l]$  and the channel state information  $\mathbf{h}_{n,k}$ . To illustrate the concept of CI, we take quadrature-PSK (QPSK) for example, and we assume  $s_{n,k}[l] = e^{j\pi/4}$  as the transmit symbol without loss of generality. The idea of CI is shown in Fig. 2, where the received noise-free signal is  $\mathbf{h}_{n,k}^H \mathbf{x}_n[l]$ ,  $\phi = \pi/\Omega$ , and the decision boundaries for the symbol  $e^{j\pi/4}$  are the positive halves of  $x$  and  $y$  axes. The transmit symbol  $s_{n,k}[l]$  can be correctly detected if the received signal  $y_{n,k}[l]$  lies in the first quadrant. In multi-user systems, the SLP approach designs  $\mathbf{x}_n[l]$  to ensure that point  $C$  lies in the constructive region, where the MUI is converted into CI that pushes the received signals away from the decision boundaries for improving multi-user communication performance.

To derive the mathematical formulation for multi-user communication QoS requirements, point  $C$  is projected onto the direction of  $\overrightarrow{OA}$  at point  $B$ . We define point  $D$  as the intersection of the extension of  $\overrightarrow{BC}$  with the boundaries of the constructive region. Then, point  $C$  in the constructive region should satisfy  $|\overrightarrow{BD}| - |\overrightarrow{BC}| \geq 0$ , which can be written as [8]

$$\Re\{\mathbf{h}_{n,k}^H \mathbf{x}_n[l] e^{-j\angle s_{n,k}[l]} - \sigma\sqrt{\Gamma_{n,k}}\} \tan \phi - \left| \Im\{\mathbf{h}_{n,k}^H \mathbf{x}_n[l] e^{-j\angle s_{n,k}[l]}\} \right| \geq 0, \quad \forall n, k, \quad (3)$$

where  $\Gamma_{n,k}$  is the signal-to-noise ratio (SNR) threshold for user  $k$  on the  $n$ -th subcarrier. Due to space limitations, the detailed derivation is omitted and readers can refer to [8]. We

utilize some fundamental linear algebra laws to reformulate (3) into an equivalent concise form:

$$\Re\{\tilde{\mathbf{h}}_{n,i}^H \mathbf{x}_n[l]\} \geq \gamma_{n,i}, \quad i = 1, 2, \dots, 2K, \quad (4)$$

where

$$\begin{aligned} \tilde{\mathbf{h}}_{n,2k}^H &\triangleq \mathbf{h}_{n,k}^H e^{-j\angle s_{n,k}} (\sin \phi + e^{-j\frac{\pi}{2}} \cos \phi), \quad \forall n, k, \\ \tilde{\mathbf{h}}_{n,2k-1}^H &\triangleq \mathbf{h}_{n,k}^H e^{-j\angle s_{n,k}} (\sin \phi - e^{-j\frac{\pi}{2}} \cos \phi), \quad \forall n, k, \\ \gamma_{n,2k} &= \gamma_{n,2k-1} \triangleq \sigma \sqrt{\Gamma_{n,k}} \sin \phi, \quad \forall n, k. \end{aligned} \quad (5)$$

In the remainder of this paper, we will employ (4) as the multi-user communication performance constraint.

### C. Radar Sensing Model

For the stationary target, the radar received echo signal  $y_n[l]$  can be quantified as [9]

$$y_n[l] = \beta e^{-j2\pi f_c \tau} \mathbf{a}^H(\theta) \mathbf{x}_n[l] e^{-j2\pi n \Delta f \tau} + z_r, \quad (6)$$

where  $z_r$  is the AWGN at the radar receiver,  $\beta \triangleq \sqrt{\frac{\sigma_{\text{RCS}} \lambda^2}{(4\pi)^3 R^4}}$  is the attenuation factor,  $\sigma_{\text{RCS}}$  is the target's radar cross section (RCS),  $\tau \triangleq 2R/c_0$  is the round-trip time delay,  $c_0$  is the speed of light, and  $\mathbf{a}(\theta) \triangleq [1, e^{j\frac{2\pi}{\lambda} d \sin(\theta)}, \dots, e^{j\frac{2\pi}{\lambda} (N_t-1) d \sin(\theta)}]^T \in \mathbb{C}^{N_t}$  is the transmit steering vector, with  $d$  denoting the antenna spacing and  $\lambda$  the wavelength. Generally, range estimation is performed by a correlator bank. Therefore, the radar ranging performance is featured by the auto-correlation of the transmit waveform:

$$r(\tau) = \int_{-\infty}^{+\infty} x(t)x^*(t-\tau)dt, \quad (7)$$

where  $x(t) = \mathbf{a}^H(\theta) \mathbf{x}(t)$  is the emitted signal through the  $N_t$  antennas. With the CP in OFDM signals, we can approximate the samples of the auto-correlation using the circular auto-correlation [10], which can be written as

$$r[m] = \sum_{p=0}^N x[p]x^*[\text{mod}(p-m, N)], \quad (8)$$

where  $m$  is range bin index,  $x[p] = x(pT_c)$ , and  $T_c = T_s/N$  is the sampling period.

It can be seen that the auto-correlation function  $r[m]$  is random due to the randomness of dual-function waveform. The random communication waveforms may lead to high range sidelobes, rendering poor ranging performance. In this paper, we employ the SLP technique to suppress the range sidelobes by elaborately designing the transmit waveform.

It is widely acknowledged that the auto-correlation with a significant peak at the mainlobe ( $m = 0$ ) and low sidelobes ( $m \neq 0$ ) offer superior radar ranging performance. However, due to the stochastic nature of the dual-function waveform, the auto-correlation  $r[m]$  is a random function. Consequently, the resulting range profile may exhibit a high range sidelobe level, thereby compromising the radar ranging performance. To overcome this drawback, we employ the SLP technique to suppress the range sidelobes by elaborately designing the

transmit waveform. The commonly used metric to quantify the sidelobe level is the ISL:

$$\xi_r = \sum_{\substack{m=-N+1 \\ m \neq 0}}^{N-1} |r[m]|^2 = 2 \sum_{m=1}^{N-1} |r[m]|^2. \quad (9)$$

However, the explicit relationship between ISL and  $\mathbf{x}_n[l]$  cannot be found from (9). Using the Parseval equality, a more intuitive analytic expression of ISL can be obtained by [11]

$$\xi_r = 2 \left( \frac{1}{N} \sum_{n=0}^{N-1} |\mathbf{a}^H \mathbf{x}_n|^4 - \left( \frac{1}{N} \sum_{n=0}^{N-1} |\mathbf{a}^H \mathbf{x}_n|^2 \right)^2 \right), \quad (10)$$

where the time-slot index  $[l]$  and angle  $\theta$  is omitted for conciseness. Since ISL indicates the self-interference from the sidelobes, the smaller the ISL, the better the radar ranging performance.

### D. Problem Formulation

To facilitate the algorithm development, we first convert the ISL (10) into an equivalent concise form:

$$\xi_r = \frac{2}{N} \tilde{\mathbf{x}}^H \mathbf{A}^H \mathbf{A} \tilde{\mathbf{x}} - \frac{2}{N^2} (\mathbf{x}^H \tilde{\mathbf{A}} \mathbf{x})^2, \quad (11)$$

where we define

$$\begin{aligned} \mathbf{x} &\triangleq [\mathbf{x}_0^T, \mathbf{x}_1^T, \dots, \mathbf{x}_{N-1}^T]^T, \quad \tilde{\mathbf{x}} \triangleq \text{vec}(\mathbf{x}\mathbf{x}^H), \\ \mathbf{a}_n &\triangleq \mathbf{e}_{n+1} \otimes \mathbf{a}, \quad \mathbf{A}_n \triangleq \mathbf{a}_n \mathbf{a}_n^H, \quad \tilde{\mathbf{A}} \triangleq \sum_{n=0}^{N-1} \mathbf{A}_n, \\ \mathbf{A} &\triangleq [\text{vec}(\mathbf{A}_0), \text{vec}(\mathbf{A}_1), \dots, \text{vec}(\mathbf{A}_{N-1})]^H, \end{aligned} \quad (12)$$

and  $\mathbf{e}_n \in \mathbb{R}^N$  indicates the  $n$ -th column of an  $N \times N$  identity matrix. We aim to design the SLP transmit waveform  $\mathbf{x}$  to minimize the ISL while satisfying the multi-user communication QoS requirements and the transmit power constraint. Therefore, the optimization problem for SLP-based low-range-sidelobe waveform design can be formulated as

$$\min_{\mathbf{x}_n, \forall n} \xi_r = \frac{2}{N} \tilde{\mathbf{x}}^H \mathbf{A}^H \mathbf{A} \tilde{\mathbf{x}} - \frac{2}{N^2} (\mathbf{x}^H \tilde{\mathbf{A}} \mathbf{x})^2 \quad (13a)$$

$$\text{s.t.} \quad \Re\{\tilde{\mathbf{h}}_{n,i}^H \mathbf{x}_n\} \geq \gamma_{n,i}, \quad \forall n, i, \quad (13b)$$

$$\sum_{n=0}^{N-1} \|\mathbf{x}_n\|^2 \leq P_0, \quad (13c)$$

where  $P_0$  is the transmit power budget. Due to the quartic objective function (13a), the optimization problem (13) cannot be easily solved via existing optimization algorithms. Therefore, we will develop an efficient algorithm utilizing the MM framework to solve the waveform design problem.

## III. PROPOSED SLP-BASED LOW-RANGE-SIDELOBE WAVEFORM DESIGN ALGORITHM

To solve the resulting non-convex waveform design problem (13) efficiently, we utilize MM framework [12] to transform the original problem into a more tractable optimization problem. In specific, we seek an upper-bound surrogate function

$$\tilde{\mathbf{x}}^H \mathbf{A}^H \mathbf{A} \tilde{\mathbf{x}} \stackrel{(a)}{\leq} \lambda_a \tilde{\mathbf{x}}^H \tilde{\mathbf{x}} + 2\Re \{ \tilde{\mathbf{x}}^H (\mathbf{A}^H \mathbf{A} - \lambda_a \mathbf{I}) \tilde{\mathbf{x}} \} + \tilde{\mathbf{x}}_t^H (\lambda_a \mathbf{I} - \mathbf{A}^H \mathbf{A}) \tilde{\mathbf{x}}_t \quad (14a)$$

$$\stackrel{(b)}{\leq} 2\Re \{ \mathbf{x}^H \mathbf{B} \mathbf{x} \} + \lambda_a P_0^2 + \tilde{\mathbf{x}}_t^H (\lambda_a \mathbf{I} - \mathbf{A}^H \mathbf{A}) \tilde{\mathbf{x}}_t \quad (14b)$$

$$\stackrel{(c)}{\leq} 2\Re \{ 2\lambda_b \mathbf{x}^H \mathbf{x} + \mathbf{x}_t^H \mathbf{B} \mathbf{x} + \mathbf{x}^H \mathbf{B} \mathbf{x}_t - 2\lambda_b \mathbf{x}^H \mathbf{x}_t + \mathbf{x}_t^H (\lambda_b \mathbf{I} - \mathbf{B}) \mathbf{x}_t \} + \lambda_a P_0^2 + \tilde{\mathbf{x}}_t^H (\lambda_a \mathbf{I} - \mathbf{A}^H \mathbf{A}) \tilde{\mathbf{x}}_t \quad (14c)$$

$$\stackrel{(d)}{\leq} 2\Re \{ \mathbf{x}^H (\mathbf{B} + \mathbf{B}^H - 2\lambda_b \mathbf{I}) \mathbf{x}_t \} + \lambda_a P_0^2 + \tilde{\mathbf{x}}_t^H (\lambda_a \mathbf{I} - \mathbf{A}^H \mathbf{A}) \tilde{\mathbf{x}}_t + 2\lambda_b P_0 + 2\Re \{ \mathbf{x}_t^H (\lambda_b \mathbf{I} - \mathbf{B}) \mathbf{x}_t \}, \quad (14d)$$

$$\stackrel{(e)}{=} 2\Re \{ \mathbf{x}^H (\mathbf{B} + \mathbf{B}^H - 2\lambda_b \mathbf{I}) \mathbf{x}_t \} + c_1, \quad (14e)$$

that locally approximates the objective function (13a) and minimize the surrogate function in each iteration. The following describes the procedure of deriving the surrogate functions for  $\tilde{\mathbf{x}}^H \mathbf{A}^H \mathbf{A} \tilde{\mathbf{x}}$  and  $(\mathbf{x}^H \tilde{\mathbf{A}} \mathbf{x})^2$ , respectively.

#### A. Majorizing $\tilde{\mathbf{x}}^H \mathbf{A}^H \mathbf{A} \tilde{\mathbf{x}}$

The upper-bound surrogate function of  $f(\mathbf{x})$  can be derived according to the second-order Taylor expansion at  $\mathbf{x}_t$  as [12]:

$$f(\mathbf{x}) \leq f(\mathbf{x}_t) + \nabla f(\mathbf{x}_t)^H (\mathbf{x} - \mathbf{x}_t) + \frac{1}{2} (\mathbf{x} - \mathbf{x}_t)^H \mathbf{M} (\mathbf{x} - \mathbf{x}_t), \quad (15)$$

where  $\mathbf{M} \succeq \nabla^2 f(\mathbf{x})$ . Inspired by (15), we can transform  $\tilde{\mathbf{x}}^H \mathbf{A}^H \mathbf{A} \tilde{\mathbf{x}}$  into a simple linear function based on the second-order Taylor expansion in steps (a) and (c), respectively. The details of the derivation are presented in (14), where  $\mathbf{B} \triangleq \sum_{n=0}^{N-1} \mathbf{A}_n \mathbf{x}_t \mathbf{x}_t^H \mathbf{A}_n^T - \lambda_a \mathbf{x}_t \mathbf{x}_t^H$ ,  $\lambda_a = \lambda_{\max} \{ \mathbf{A}^H \mathbf{A} \}$  and  $\lambda_b = \lambda_{\max} \{ \mathbf{B} \}$  are the maximum eigenvalues of matrices  $\mathbf{A}^H \mathbf{A}$  and  $\mathbf{B}$ , respectively, and the constant term  $c_1$  is irrelevant to variable  $\mathbf{x}$ . With the transmit power constraint (13c), step (b) is obtained by  $\tilde{\mathbf{x}}^H \tilde{\mathbf{x}} = \text{vec}^H(\mathbf{x} \mathbf{x}^H) \text{vec}(\mathbf{x} \mathbf{x}^H) \leq P_0^2$ . Similarly, step (d) is derived using  $\mathbf{x}^H \mathbf{x} \leq P_0$ .

However, calculating the maximum eigenvalue  $\lambda_a$  of the matrix  $\mathbf{A}^H \mathbf{A}$  with the dimension  $N^2 N_t^2 \times N^2 N_t^2$  is computationally challenging. To tackle this issue, we exploit the unique signal structures and find that  $\lambda_a$  is a constant that depends only on the number of transmit antennas. Recalling the definition given in (12), we can obtain that  $\mathbf{A}^H \mathbf{A} = \sum_{n=0}^{N-1} \mathbf{A}_n \otimes \mathbf{A}_n$  and  $\mathbf{A}_n^H \mathbf{A}_{n'} = \mathbf{0}, \forall n \neq n'$ . Since  $\mathbf{A}_n$  is a Hermitian matrix, the eigenvectors of  $\mathbf{A}_n$  and  $\mathbf{A}_{n'}$  are orthogonal. Therefore, we can directly obtain the value of  $\lambda_a$  as

$$\begin{aligned} \lambda_a &= \max_{n=0,1,\dots,N-1} \lambda_{\max} \{ \mathbf{A}_n \otimes \mathbf{A}_n \} \\ &= \max_{n=0,1,\dots,N-1} \lambda_{\max}^2 \{ (\mathbf{e}_{n+1} \otimes \mathbf{a})(\mathbf{e}_{n+1} \otimes \mathbf{a}^H) \} \\ &= \max_{n=0,1,\dots,N-1} \lambda_{\max}^2 \{ (\mathbf{e}_{n+1} \mathbf{e}_{n+1}^H) \otimes (\mathbf{a} \mathbf{a}^H) \} \\ &= N_t^2. \end{aligned} \quad (16)$$

In this way, we can substantially reduce the computational complexity in majorizing  $\tilde{\mathbf{x}}^H \mathbf{A}^H \mathbf{A} \tilde{\mathbf{x}}$ . Subsequently, we need to derive the lower-bound surrogate function of  $(\mathbf{x}^H \tilde{\mathbf{A}} \mathbf{x})^2$ .

#### B. Minorizing $(\mathbf{x}^H \tilde{\mathbf{A}} \mathbf{x})^2$

It is easy to prove that  $(\mathbf{x}^H \tilde{\mathbf{A}} \mathbf{x})^2$  is a convex function with respect to  $\mathbf{x}$  by showing that the Hessian matrix  $\nabla^2 (\mathbf{x}^H \tilde{\mathbf{A}} \mathbf{x})^2$

---

#### Algorithm 1 Proposed SLP-based Low-Range-Sidelobe Waveform Design Algorithm

---

**Input:**  $\mathbf{h}_{n,k}, \Gamma_{n,k}, s_{n,k}, \forall n, k, \mathbf{a}(\theta), L, \phi, P_0, \delta_{\text{th}}$ .

**Output:**  $\mathbf{x}^*$ .

- 1: Initialize  $t := 0$ , initialize  $\mathbf{x}$ .
  - 2: Construct  $\mathbf{a}_n, \mathbf{A}_n, \forall n, \tilde{\mathbf{A}}, \mathbf{A}, \mathbf{x}, \tilde{\mathbf{x}}$  by (12).
  - 3: Calculate the objective value  $\xi_r$  by (13a).
  - 4: Set  $\delta := 1$ .
  - 5: **while**  $\delta \geq \delta_{\text{th}}$  **do**
  - 6:     $\hat{\xi}_r := \xi_r$ .
  - 7:    Update  $\mathbf{b}$  by (19).
  - 8:    Update  $\mathbf{x}_{t+1}$  by solving the problem (20).
  - 9:    Calculate the objective value  $\xi_r$  by (13a).
  - 10:     $\delta := |(\xi_r - \hat{\xi}_r)/\xi_r|$ .
  - 11:     $t := t + 1$
  - 12: **end while**
  - 13: Return  $\mathbf{x}^* = \mathbf{x}_t$ .
- 

is positive semi-definite. Therefore, the lower-bound surrogate function of  $(\mathbf{x}^H \tilde{\mathbf{A}} \mathbf{x})^2$  can be derived according to the first-order Taylor expansion as

$$\begin{aligned} (\mathbf{x}^H \tilde{\mathbf{A}} \mathbf{x})^2 &\geq (\mathbf{x}_t^H \tilde{\mathbf{A}} \mathbf{x}_t)^2 + 4(\mathbf{x}_t^H \tilde{\mathbf{A}} \mathbf{x}_t) \mathbf{x}_t^H \tilde{\mathbf{A}} (\mathbf{x} - \mathbf{x}_t) \\ &\quad + 4(\mathbf{x}_t^H \tilde{\mathbf{A}} \mathbf{x}_t) \mathbf{x}_t^T \tilde{\mathbf{A}}^T (\mathbf{x}^* - \mathbf{x}_t^*) \quad (17) \\ &= 8\alpha \Re \{ \mathbf{x}^H \tilde{\mathbf{A}} \mathbf{x}_t \} - 7\alpha^2, \end{aligned}$$

where  $\alpha \triangleq \mathbf{x}_t^H \tilde{\mathbf{A}} \mathbf{x}_t$  for conciseness.

Therefore, substituting (14) and (17) into objective function (13a) leads to the following inequality

$$\xi_r \leq \Re \{ \mathbf{x}^H \mathbf{b} \} + \varepsilon, \quad (18)$$

where  $\varepsilon$  is a constant term and

$$\mathbf{b} \triangleq \frac{4}{N} (\mathbf{B} + \mathbf{B}^H - 2\lambda_b \mathbf{I}) \mathbf{x}_t - \frac{16\alpha}{N^2} \tilde{\mathbf{A}} \mathbf{x}_t. \quad (19)$$

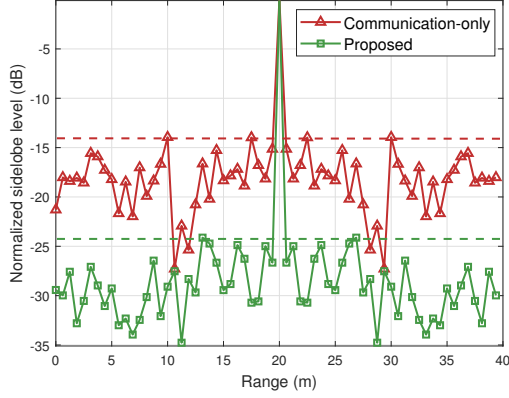
By ignoring the constant term  $\varepsilon$ , the optimization problem in each iteration can be formulated as

$$\min_{\mathbf{x}_n, \forall n} \Re \{ \mathbf{x}^H \mathbf{b} \} \quad (20a)$$

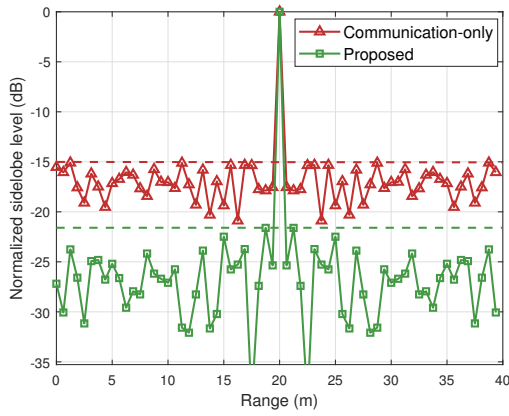
$$\text{s.t.} \quad \Re \{ \tilde{\mathbf{h}}_{n,i}^H \mathbf{x}_n \} \geq \gamma_{n,i}, \forall n, i, \quad (20b)$$

$$\sum_{n=0}^{N-1} \|\mathbf{x}_n\|^2 \leq P_0. \quad (20c)$$

It can be seen that the optimization problem (20) is convex, which can be easily solved by various existing convex opti-



(a) Radar range profile for the  $K = 3$  scenario.



(b) Radar range profile for the  $K = 4$  scenario.

Fig. 3: Radar range profiles for a target at 20m,  $\Gamma = 6$ dB,  $L = 50$ .

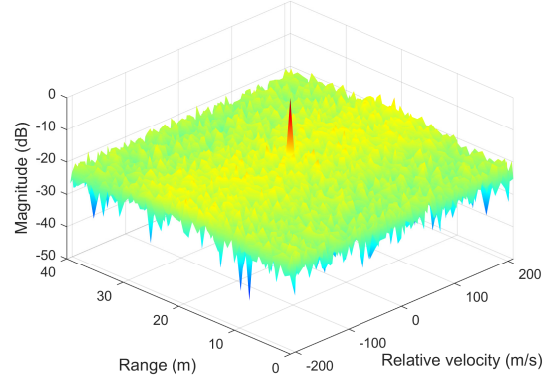
mization algorithm.

With the above derivations, the proposed SLP-based low-range-sidelobe waveform design algorithm is summarized in Algorithm 1, where  $\delta_{th}$  represents the convergence threshold. In summary, the SLP transmit waveform  $\mathbf{x}$  is iteratively optimized by solving the problem (20) until convergence.

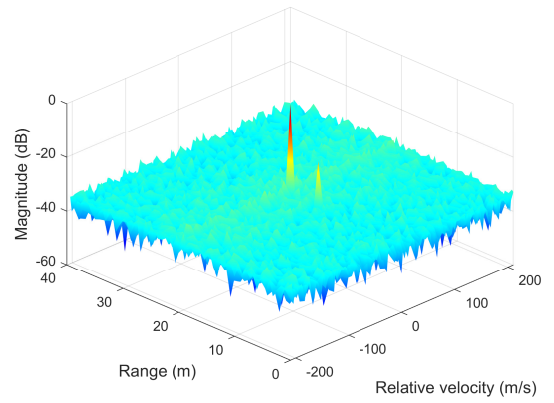
#### IV. SIMULATION RESULTS

In this section, we provide numerical results to evaluate the performance of the proposed SLP-based low-range-sidelobe waveform design for ISAC systems. Without loss of generality, we assume that the BS is equipped with  $N_t = 8$  antennas with antenna spacing  $d = \lambda/2$ . The number of subcarriers is  $N = 64$ , the CP length is  $N_{CP} = N/4$ . The communication noise power is  $\sigma^2 = 10$ dBm, and the QoS requirements are identical for each subcarrier and communication user, i.e.,  $\Gamma = \Gamma_{n,k}$ . In addition, the transmit power is  $P_0 = 0.5$ W and the convergence threshold is set as  $\delta_{th} = 10^{-5}$ .

To validate the performance of the proposed SLP-based low-range-sidelobe waveform design in terms of range sidelobe suppression, we employ the proximate matched filter with



(a) Communication-only waveform.



(b) Proposed waveform.

Fig. 4: The range-Doppler map for two stationary targets at ranges 15m and 20m, respectively,  $\Gamma = 6$ dB,  $L = 256$ .

circular correlation (PMF-CC) [10] commonly used in OFDM radar to achieve the range profile. The radar range profiles of different waveforms are shown in Fig. 3. The communication-only waveform is obtained by minimizing the transmitted power under the communication QoS requirements. It can be seen that the proposed waveform achieves a 10dB range sidelobe reduction for the  $K = 3$  scenario and a 7dB range sidelobe reduction for the  $K = 4$  scenario compared with the communication-only waveform, which improves the radar ranging performance while maintaining satisfactory communication QoS.

Next, we demonstrate the radar ranging performance of the proposed SLP-based low-range-sidelobe waveform design in a multi-target scenario. The range-Doppler map is also achieved by PMF-CC in [10]. In Fig. 4, a strong target with  $\sigma_{RCS} = 20$ dBsm (e.g. car) and a weak target with  $\sigma_{RCS} = 1$ dBsm (e.g. pedestrian) are simulated at nearby ranges. For the communication-only waveform, the weak target at 15m is likely to be submerged in the sidelobes of the strong target at 20m, which makes it difficult to be detected. By contrast, for the proposed waveform, the mainlobe level of the weak target

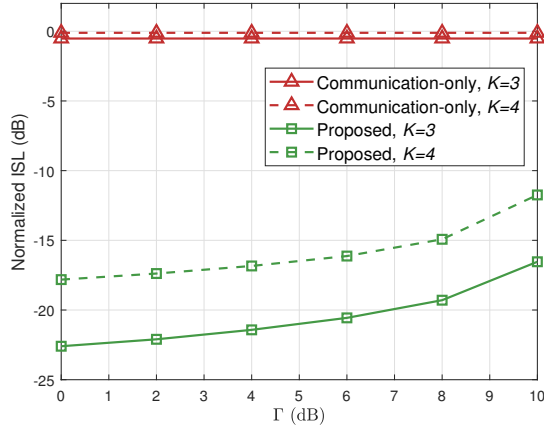


Fig. 5: The ISL of different waveforms versus the communication QoS requirements  $\Gamma$ .

is much higher than the sidelobe level so that it can be detected easily. Therefore, the proposed SLP-based low-range-sidelobe waveform design can achieve better radar ranging performance by suppressing the range sidelobes.

Furthermore, Fig. 5 evaluates the ranging performance of different waveforms in terms of the ISL. Compared with the communication-only waveform, the proposed SLP-based low-range-sidelobe waveform design can significantly reduce the ISL of transmit waveform by exploiting more DoFs in the temporal domain, improving the radar ranging performance. Besides, the ISL of the proposed waveform increases with larger  $\Gamma$  and  $K$ , which demonstrates the performance trade-off between multi-user communication and radar sensing.

Finally, in order to further investigate the impact of range sidelobes on radar ranging performance, we analyze the range estimation root mean square error (RMSE) of the weak target for the case that we attempt to estimate the range of two distinct targets with different RCS. The strong target is located at 20m with  $\sigma_{\text{RCS}} = 20\text{dBsm}$ , while the weak target is randomly distributed between 20m to 25m with  $\sigma_{\text{RCS}} = 1\text{dBsm}$ . From Fig. 6, as the communication QoS requirements  $\Gamma$  and the number of communication users  $K$  increase, the RMSE of range estimation gradually increases, which further illustrates the trade-off between radar ranging performance and communication QoS. Additionally, our proposed waveform always provides better range estimation performance than the communication-only waveform by suppressing range sidelobes. This demonstrates the superiority of the proposed SLP-based low-range-sidelobe waveform design for range estimation and the effectiveness of utilizing ISL as the sensing performance metric.

## V. CONCLUSIONS

In this paper, we proposed an SLP-based low-range-sidelobe waveform design for an MIMO-OFDM ISAC system. The ISL of the transmit waveform was minimized while satisfying the multi-user communication QoS requirements and the transmit

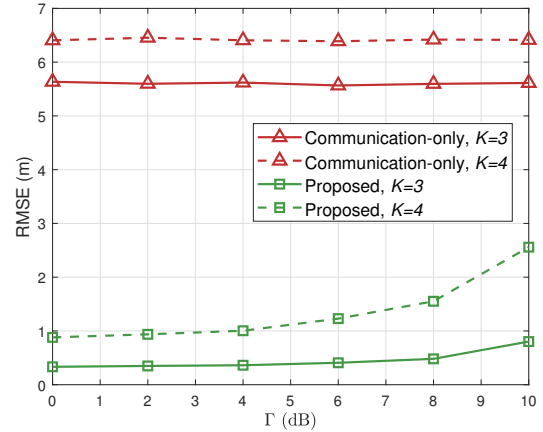


Fig. 6: Range estimation RMSE of the weak target versus the communication QoS requirements  $\Gamma$ .

power constraint. We developed an efficient algorithm utilizing MM framework to solve the waveform design problem. Simulation results were provided to reveal radar ranging performance improvement and demonstrated the benefits of the proposed SLP-based low-range-sidelobe waveform design in ISAC systems.

## REFERENCES

- [1] Y. Cui, F. Liu, X. Jing, and J. Mu, "Integrating sensing and communications for ubiquitous IOT: Applications, trends, and challenges," *IEEE Network*, vol. 35, no. 5, pp. 158-167, Sep. 2021.
- [2] R. Liu, M. Li, Q. Liu, and A. L. Swindlehurst, "Dual-functional radar-communication waveform design: A symbol-level precoding approach," *IEEE J. Sel. Topics Signal Process.*, vol. 15, no. 6, pp. 1316-1331, Nov. 2021.
- [3] L. Chen, Z. Wang, Y. Du, Y. Chen, and F. R. Yu, "Generalized transceiver beamforming for DFRC with MIMO radar and MU-MIMO communication," *IEEE J. Sel. Areas Commun.*, vol. 40, no. 6, pp. 1795-1808, Jun. 2022.
- [4] B. Tang, H. Wang, L. Qin, and L. Li, "Waveform design for dualfunction MIMO radar-communication systems," in *Proc. IEEE Sensor Array Multichannel Signal Process. Workshop (SAM)*, Hangzhou, China, Jun. 2020.
- [5] P. Kumari, S. A. Vorobyov, and R. W. Heath, "Adaptive virtual waveform design for millimeter-wave joint communication-radar," *IEEE Trans. Signal Process.*, vol. 68, pp. 715-730, Nov. 2019.
- [6] J. Song, P. Babu, and D. P. Palomar, "Sequence design to minimize the weighted integrated and peak sidelobe levels," *IEEE Trans. Signal Process.*, vol. 64, no. 8, pp. 2051-2064, Apr. 2016.
- [7] H. Li, W. Cai, Y. Liu, M. Li, Q. Liu, and Q. Wu, "Intelligent reflecting surface enhanced wideband MIMO-OFDM communications: From practical model to reflection optimization," *IEEE Trans. Commun.*, vol. 69, no. 7, pp. 4807-4820, Jul. 2021.
- [8] R. Liu, M. Li, Q. Liu, and A. L. Swindlehurst, "Joint waveform and filter designs for STAP-SLP-based MIMO-DFRC systems," *IEEE J. Sel. Areas Commun.*, vol. 40, no. 6, pp. 1918-1931, Jun. 2022.
- [9] C. Sturm and W. Wiesbeck, "Waveform design and signal processing aspects for fusion of wireless communications and radar sensing," *IEEE Proc.*, vol. 99, no. 7, pp. 1236-1259, Jul. 2011.
- [10] S. Mercier, S. Bidon, D. Roque, and C. Enderli, "Comparison of correlation-based OFDM radar receivers," *IEEE Trans. Aerosp. Electron. Syst.*, vol. 56, no. 6, pp. 4796-4813, Dec. 2020.
- [11] H. Li, "Frequency multiplexing and waveform synthesis in joint communications and sensing," in *Proc. IEEE Wireless Commun. Netw. Conf. (WCNC)*, Austin, TX, Apr. 2022.
- [12] Y. Sun, P. Babu, and D. P. Palomar, "Majorization-minimization algorithms in signal processing, communications, and machine learning," *IEEE Trans. Signal Process.*, vol. 65, no. 3, pp. 794-816, Feb. 2017.